

Cyto- and genotoxicity assessment of Gold nanoparticles obtained by laser ablation in A549 lung adenocarcinoma cells

Sebastiano Di Bucchianico · Lucia Migliore ·
Paolo Marsili · Chiara Vergari ·
Francesco Giammanco · Emilia Giorgetti

Received: 15 December 2014 / Accepted: 29 April 2015 / Published online: 12 May 2015
© Springer Science+Business Media Dordrecht 2015

Abstract Gold nanoparticles have attracted enormous interest in biomedical applications, based on their unique optical properties. However, their toxicity on human tissues is still an open issue. Beyond the potential intrinsic toxicity of nanostructured gold, a non-negligible contribution of stabilizers or reaction by-products related to current wet chemical synthesis procedures can be expected. Aimed at isolating gold contribution from that of any other contaminant, we produced colloidal suspensions of Gold nanoparticles having average size <10 nm in deionized water or

acetone by pulsed laser ablation, that permits preparation of uncoated and highly stable Gold nanoparticles in pure solvents. Subsequently, we investigated the role of surface chemistry, size, and dispersivity of synthesized Gold nanoparticles in exerting toxicity in a cell model system of deep respiratory tract, representing the main route of exposure to NPs, namely adenocarcinoma epithelial A549 cells. Gold nanoparticles prepared in water showed no particular signs of cytotoxicity, cytostasis, and/or genotoxicity as assessed by MTT colorimetric viability test and Cytokinesis-block micronucleus cytochrome assay up to concentrations of the order of 5 $\mu\text{g/mL}$. In contrast, Gold nanoparticles produced in pure acetone and then transferred into deionized water showed impaired cell viability, apoptosis responses, micronuclei, and dicentric chromosomes induction as well as nuclear budding, as a function of the amount of surface contaminants like amorphous carbon and enolate ions.

S. Di Bucchianico · L. Migliore
Department of Translational Research and New Technologies in Medicine and Surgery, Division of Medical Genetics, University of Pisa, Pisa, Italy

Present Address:
S. Di Bucchianico
Institute of Environmental Medicine, Karolinska Institutet, Stockholm, Sweden

P. Marsili · E. Giorgetti (✉)
Institute of Complex Systems (ISC-CNR), Via Madonna del Piano 10, 50019 Sesto Fiorentino (Firenze), Italy
e-mail: emilia.giorgetti@fi.isc.cnr.it

P. Marsili · F. Giammanco
Department of Physics “E. Fermi”, University of Pisa, Pisa, Italy

C. Vergari
Plasma Diagnostics and Technologies s.r.l., Largo B. Pontecorvo 3, Pisa, Italy

Keywords Au nanoparticles · Pulsed laser ablation · Cytotoxicity · Genotoxicity · Biomedicine · Health effects

Introduction

A handful of nanomaterials are being studied in clinical trials or have already been approved for use in humans (Peer et al. 2007; McCarthy et al. 2005; Davis

et al. 2010), and many proof-of-concept studies of nanomaterials in cell cultures and small animal models for medical applications are under way (Resch-Genger et al. 2008; Sperling et al. 2008; Liu et al. 2008). Among the experimented nanomaterials, gold is undoubtedly one of the most used, having its first medical application dating back to several centuries ago (Dreaden et al. 2012; Dykman and Khlebtsov 2012). When reduced to the nanoscale in the form of spheres, cages, stars, or rods and functionalized by different molecular coatings, this metal seems particularly attractive for the development of a plenty of innovative diagnostic and therapeutic processes, which take advantage of its extraordinary properties. Indeed, the range of uses of Au nanoparticles (NPs) in current medical and biological research is extremely broad and include diagnostics, therapy, prophylaxis, and hygiene (Dykman and Khlebtsov 2012). However, their possible toxicity is still an open issue.

Conventional AuNPs are usually generated by wet chemical methods (Turkevich et al. 1953; Demartini et al. 2009; Trigari et al. 2011). For such AuNPs, an increasing number of studies is available on induced in vitro and in vivo genotoxic and cytotoxic effects but the toxicological profile of AuNPs remains controversial. Factors such as shape, size, and surface properties and coatings are known to affect the AuNPs physicochemical characteristics eventually influencing their uptake and toxicity (Alkilany and Murphy 2010; Liu et al. 2014). In a series of in vitro cell models, AuNPs induced apoptosis and mitochondrial damage via oxidative stress mechanisms, as well as actin and tubulin cytoskeleton disturbance, resulting in reduced cell proliferation and cellular differentiation (Pan et al. 2009; Soenen et al. 2012; Söderstjerna et al. 2014). Apoptosis, aneuploidy, and both DNA damage and oxidation play a pivotal role in the cytotoxicity and genotoxicity exerted by differently sized AuNPs (Paino et al. 2012; Di Bucchianico et al. 2014). Moreover, transplacental size-dependent clastogenic and epigenetic effects of AuNPs in mouse fetus was also noticed as well as in vitro genomic instability and chromatin condensation (Li et al. 2011; Schaeublin et al. 2012; Balansky et al. 2013).

In general, it seems that residues of precursors and stabilizing agents in the final products are the ones mainly responsible for the observed toxicity (Connor et al. 2005; Uboldi et al. 2009), and a “safety by design” approach is proposed in an EU-funded

research project, Sanowork, in order to establish a primary prevention of NPs potential risks (www.sanowork.eu). However, the available data do not permit a reliable discrimination between the intrinsic effect of nanostructured Gold and that of surface coatings or reaction by-products.

In recent years a lot of interest has been devoted to a physical process, namely pulsed laser ablation (PLAL) in liquids that, under proper working conditions, permits preparation of uncoated and highly stable AuNPs in pure solvents (Zeng et al. 2012). Such NPs can consequently be considered as a model system to isolate the toxicity (if any) of nanosized Au from that of other contaminants. While, to our knowledge, no studies on genotoxicity are available, a few studies evaluated the toxicity of AuNPs prepared by PLAL (Kim et al. 2012; Jeong et al. 2013; Taylor et al. 2010; Salmaso et al. 2009). In particular, no toxic effects were detected after treatment of human breast adenocarcinoma MCF7 cells with concentrations up to 0.74 nM (0.15 µg/mL) of 18 nm size PLAL-prepared AuNPs (Salmaso et al. 2009). Higher NPs concentrations were tested on bovine-immortalized endothelial cell line GM7373 and no significant toxicity was observed using 15 nm size AuNPs up to 0.5 µg/mL concentrations (Taylor et al. 2010). More recently, it has been shown that AuNPs having 20–30 nm size and prepared by PLAL in aqueous solution are biocompatible and safe, up to 10,000 µg/mL for 72 h, as evaluated by analyzing cell survival and cell morphology. These NPs were internalized through endocytosis in glioblastoma and neuroblastoma human cell lines, independent of synthesis solutions and/or size (Correard et al. 2014).

Therefore, our study is aimed at deepening the present poor knowledge of the effect of PLAL-prepared AuNPs on human cell cultures, by examining, as a function of Au concentration, the cytotoxicity, cytostasis, and genotoxicity and the role of surface chemistry, size, and dispersivity of PLAL-synthesized AuNPs, having average diameter <10 nm. We chose the human pulmonary epithelial cell line A549, a cell model system of deep respiratory tract, representing the main route of exposure to NPs. To this aim, we exposed A549 cells to various concentrations of AuNPs prepared by PLAL in different experimental conditions. PLAL settings were tuned in order to achieve different size, dispersivity, or surface properties and hence to unveil the role of these

parameters on the occurrence of cyto- and genotoxic effects. In particular, AuNPs were prepared in pure deionized water or pure acetone (and subsequently transferred to water). Depending on the preparation conditions, they exhibited different mean size (2–7 nm) and, in some cases, the presence of traces of amorphous carbon or enolate ions on their surface. Cell viability was determined by MTT (methylthiazol tetrazolium) assay, based on the measurement of the mitochondrial dehydrogenase activity of cells. Cytotoxicity and cytostasis were morphologically evaluated via apoptotic and necrotic cell ratios and via the proportion of mono-, bi-, and multinucleated cells in cytochalasin B-treated cultures, respectively while genotoxicity was assessed by cytokinesis-block micronucleus cytome assay (CBMN Cyt). This comprehensive system was used for measuring chromosomal damage events like micronuclei induction, a biomarker of chromosome breakage and/or whole chromosome loss, nucleoplasmic bridges formation, a sensitive measure of chromosome rearrangement, and nuclear buds generation, a biomarker of elimination of amplified DNA and/or DNA repair complexes.

Experimental methods

Laser ablation

We prepared colloidal suspensions of AuNPs in deionized water (18.2 M Ω cm @ 25 °C) or acetone (Carlo Erba >99.8 %). The AuNPs were obtained by PLAL of a gold target in liquid environment with the fundamental (1064 nm) or the second harmonic (532 nm) of a mode-locked Nd-YAG laser (EKSPALA PL2143A: rep. rate 10 Hz, pulse width 25 ps at 1064 nm and 20 ps at 532 nm). The laser beam was focused with a lens having 20 cm focal length. The target was placed at the bottom of a 1 cm \times 1 cm quartz cuvette and was kept 2 cm in front of the focal plane. The diameter of the laser spot on the target was fixed at 1 mm. The volume of the solvent used for the ablation and post-irradiation tests was 2 mL, corresponding to a 2-cm-high liquid column. The pulse energy was 15 mJ in the case of ablation in acetone. It corresponds to a fluence (i.e., energy per unit surface) on target of \approx 2 J/cm², and 30 mJ in the case of ablation in water. In the latter case, due to the absorption of water at 1064 nm, the corresponding

fluence on target is of \approx 1.5 J/cm². The ablation process was monitored by measuring in situ the visible spectra with an Avantes fiber spectrophotometer and a deuterium–tungsten lamp. The sampling beam was perpendicular to the ps laser beam and crossed the quartz cuvette 0.5 cm above the bottom of the cell.

The gold target was purchased from Goodfellow (high purity: 99.95 %).

We transferred the AuNPs obtained in pure acetone into deionized water, by following the procedure previously described (Giorgetti et al. 2012). Basically, we added deionized water to the colloids (2:1 acetone/water volume ratio) and let acetone to evaporate. The operation was repeated several times, until no trace of acetone absorption was observed in the UV region of the colloid electronic spectrum. We performed phase transfer at room temperature under fume hood. The process typically takes several hours.

TEM samples were obtained by dropping a small amount of colloid onto carbon-coated copper grids and letting it to evaporate. The images were recorded with a Philips CM12, 120 kV. Particle mean diameter and dispersivity were determined by fitting the measured statistical distributions with a lognormal function. This permits calculation of NPs and Au concentration by fitting the experimental UV–Vis spectra of the colloids with a home-made computer code, based on first-order Mie Scattering theory (Giorgetti et al. 2011, 2009; Haiss et al. 2007; Giorgetti et al. 2006).

HRTEM imaging and EDX microanalysis were performed with a HRTEM JEOL2010, 200 kV. The ζ -potential of the colloids in water was measured with a Zetasizer Nano ZS90, Malvern Instruments.

Cell culture and Au exposure

Human lung adenocarcinoma epithelial A549 cells were purchased, mycoplasma free, from the Istituto Zooprofilattico of Brescia (Italy). The cells were cultured in Ham's F12 Medium with L-glutamine (Lonza, Italy) supplemented with 10 % fetal bovine serum of South American origin (Lonza, Italy) and 1 % (v/v) Penicillin (10,000 U/mL) and Streptomycin (10,000 μ g/mL) (Lonza, Italy). The cell cultures were maintained under standard conditions in a humidified atmosphere (5 % CO₂) at 37 °C and passaged weekly in tissue culture-treated flasks (Sarstedt, Italy).

Three batches of AuNPs (B1, B2, and B3) were prepared as aqueous stock solutions at the nominal

concentrations of 44, 46, and 53 $\mu\text{g/mL}$, respectively. After 24 h of seeding, the cell cultures were treated with different mass concentrations of Au in the form of AuNPs, ranging from 0.0046 to 4.6 $\mu\text{g/mL}$ and obtained from B1, B2, and B3 by diluting suitable aliquots of AuNPs stock solutions in complete culture medium.

Cell viability

The MTT (methylthiazol tetrazolium) colorimetric assay was used as cell viability test. Subconfluent A549 cells were grown in 96-well plates (Sarstedt, Italy) and exposed to AuNPs suspensions for 48 h (6 well/condition). After the exposure, medium was taken away and cells were washed twice with 100 μL PBS (Lonza, Italy) supplemented with 2 % (v/v) fetal bovine serum of South American origin (Lonza, Italy) and 1 % (v/v) Penicillin (10,000 U/mL) and Streptomycin (10,000 $\mu\text{g/mL}$) (Lonza, Italy). 10 μL of a 5 mg/mL MTT solution (3-(4,5-dimethylthiazolyl-2)-2, 5-diphenyltetrazolium bromide; Sigma-Aldrich, Italy) was added to 90 μL of complete cell medium (nine wells for each condition). After 3 h at 5 % CO_2 and 37 °C, A549 medium was replaced by 100 μL of dimethyl sulfoxide (DMSO; Sigma-Aldrich, Italy) and mixed thoroughly to dissolve the formazan crystals. To limit potential interactions due to the presence of residual NPs that could interfere with the assay, blanks without cells were used to detect the absorption of AuNPs themselves (3 well/condition). Absorbance was measured at 570 nm (630 nm background) and cell viability was determined as the percentage of the blanks subtracted from the corresponding percentage of the exposed cells. 1 mM sodium chromate (Sigma-Aldrich, Italy) was used as positive control.

CBMN Cyt assay

Cytokinesis-block micronucleus cytochrome (CBMN cyt) assay was performed as already described (Di Bucchianico et al. 2013). Briefly, 7×10^4 A549/well were plated onto 6-well plates (Sarstedt, Italy) and 24 h after seeding the cells were exposed, for 48 h, to the three batches of AuNPs (B1, B2, and B3) as described above and to 0.10 $\mu\text{g/mL}$ Mitomycin C (Sigma-Aldrich, Italy) as positive control according to OECD guideline 474. To block the cytokinesis process, 20 h

after exposure to the test compounds the A549 cultures were supplemented with 6 $\mu\text{g/mL}$ Cytochalasin B (Sigma-Aldrich, Italy) and then further incubated under standard cell culture conditions. At the end of the exposure period (48 h), cells were harvested and the cell pellet was subjected to hypotonic treatment (0.075 M KCl) and fixed with acetic acid–methanol (1:6) (Carlo Erba, Italy).

As described by Fenech, 500 cells were scored to evaluate the percentage of mono-, bi-, and multinucleated cells, and the cytokinesis-block proliferation index (CBPI) was calculated as an index of cytostasis by comparing the distribution of mono-, bi-, and multinucleated cells in the treated and control cells (Fenech 2007). The number of apoptotic, necrotic, and mitotic cells per 500 cells was also scored to evaluate the cytotoxicity of AuNPs.

The genotoxic potential of AuNPs was evaluated by scoring the binucleated/micronucleated cell frequency as number of 1000 binucleated cells containing one or more micronuclei (MN), a cytogenetic biomarker of chromosomal damage. Finally, on these 1000 binucleated cells other parameters such as nucleoplasmic bridges (NPB), a biomarker of DNA misrepair and/or telomere end fusions, and nuclear buds (NBUD), a biomarker of elimination of amplified DNA and/or DNA repair complexes, were also scored.

Results

Nanoparticle characterization

We performed toxicity tests using three batches of AuNPs, whose characteristics are summarized in Table 1.

We prepared batch B1 by 532 nm laser ablation in pure acetone and subsequently transferred it to water as described (Giorgetti et al. 2012). The procedure adopted for the preparation of batch B1 corresponds to the experimental conditions that guarantee the most stable samples, the smallest particle size, and the narrowest statistical distribution that can be obtained with our experimental set up. However, the presence on NPs surface of traces of amorphous carbon and of enolate ions, which provide the extraordinary stabilization mechanism, could contribute to particle toxicity (Giorgetti et al. 2012). In order to reduce the amount of contaminants, we prepared a second batch

Table 1 Summary of AuNPs characteristics

Batch	Solvent	Ablation wavelength (nm)	Fluence on target (J/cm^2)	2R (σ_+/σ_-) (nm) before mixing	2R (σ_+/σ_-) (nm) after mixing	C_{Au} ($\mu g/mL$)	C_{NP} (NP/cc)	ζ -potential (mV)
B1	Acetone and subsequent transfer to water	532	1.9	2.3 (+1/-0.7)	2.7 (+1.8/-1.1)	44	2×10^{14}	-23 ± 8
B2	Water	1064	1.5	7.1 (+5.4/-3)	Not significant number of NPs	46	4×10^{12}	-43 ± 12
B3	Acetone and subsequent transfer to water	1064	1.9	2.4 (+2/-0.8)	Not significant number of NPs	53	10^{14}	-31 ± 13

R: NPs radius; σ_+ and σ_- : right and left side $1/e$ half width of NPs size statistical distribution; C_{Au} and C_{NP} : Au and NPs concentration per unit volume; ζ : z-potential

in acetone (B3), by ablation with a different wavelength, namely 1064 nm. This batch did not contain any detectable quantities of enolate, although it still contained some graphitic carbon, as observed under Raman inspection (data not shown). Indeed, being graphitic carbon and enolate the product of photodecomposition of solvent, it is reasonable to expect that both a shorter wavelength and its resonance with the plasmon band of the AuNPs, which causes a strong field confinement at surface, make 532 nm radiation more active in the production of the previous contaminants (Giorgetti et al. 2006).

In order to thoroughly exclude any enolate or graphitic carbon contribution to NPs toxicity, we also tested a batch obtained directly in pure water, namely batch B2. The stability requirements of the toxicity tests forced us to perform the ablation in water with 1064 nm. In fact, although 532 nm ablation with ps pulses permits fabrication of AuNPs in water with narrow statistical distribution and small size, their stability is weak and difficult to control (data not shown here). Such reduced stability is probably due to perturbation of the surface electrostatic equilibrium which, under interaction among 532 nm ps pulses and Au, is modified by multiphoton electron ejection (Giusti et al. 2007; Giammanco et al. 2010). In contrast, 1064 nm ablation of Au in pure water leads to stable colloids, although at the expense of dispersivity.

Figure 1a shows the UV-Vis spectrum of sample B1 before (red line) and after phase transfer to water

(blue line). During the phase transfer, we doubled the colloid concentration, as confirmed by the absorption in the plasmon peak, which is twice that of the native colloid. Figure 1b shows a typical TEM micrograph of colloid B1 after phase transfer. The inset shows a magnification of a pair of NPs in high resolution mode. Lattice planes are clearly visible, demonstrating that the NPs are crystalline. The statistical distribution of particle size is also reported in the figure. The lognormal function (red line) which gives the best fit of the statistical distribution can be described more intuitively with an asymmetric Gaussian with $R = 1.15$ nm radius peak value and $\sigma_- = 0.35$ nm and $\sigma_+ = 0.5$ nm left and right $1/e$ half width, respectively. These parameters, which are reported in Table 1, were introduced in a home-made Mie fitting routine, which returns the theoretical spectrum (black line in Fig. 1a) and the corresponding concentration of AuNPs ($C_{NP} = 2 \times 10^{14}$ NPs/cc) and, from that, the total concentration of Au in the colloid ($C_{Au} = 44 \mu g/mL$).

The same characterization was performed for batch B2. The UV-Vis spectrum of the fresh colloid is reported in Fig. 2a (red line), while Fig. 2b shows a TEM image with the corresponding statistical distribution of particle size. In this case, the best fitting parameters of the Gaussian equivalent of the lognormal distribution were $R = 3.5$ nm, $\sigma_- = 1.5$ nm, and $\sigma_+ = 2.7$ nm (Table 1). As expected, particle size distribution is much wider than in batch B2, along with

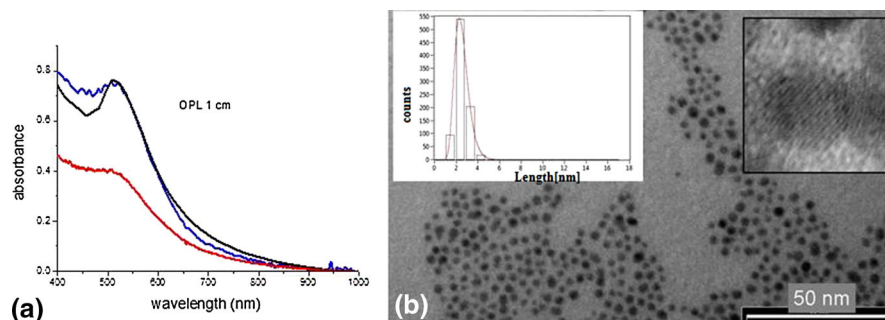
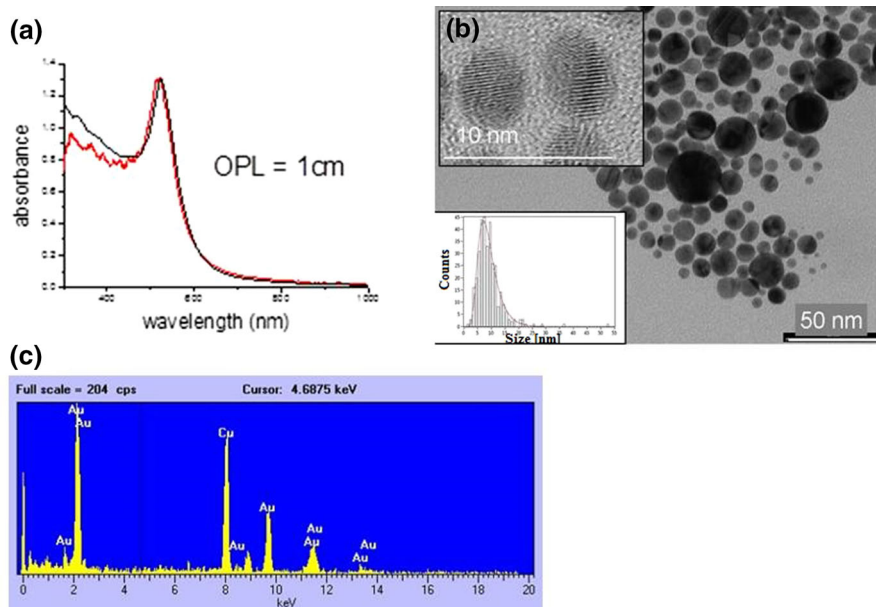


Fig. 1 **a** UV-Vis spectra of sample B1 before (*red line*) and after (*blue line*) transfer to water. The *black line* represents the theoretical fit of the spectrum, that permitted evaluation of gold and of AuNPs concentration. Optical path length

(OPL) = 1 cm. **b** Typical TEM image of sample B1, with statistical distribution of particle size and high resolution magnification (*inset*). (Color figure online)

Fig. 2 **a** UV-Vis spectrum of sample B2 (*red line*) and theoretical fit (*black line*). OPL = 1 cm. **b** Typical TEM image of sample B2 with statistical distribution of particle size and high resolution imaging of a couple of NPs (*inset*). **c** EDX spectra. (Color figure online)

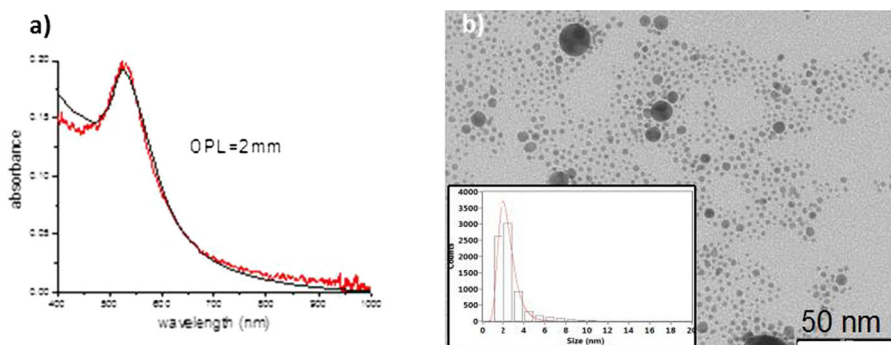


NPs diameter, which is more than doubled. The theoretical best fitting spectrum for this batch is also reported in Fig. 2a (black line) and returns a concentration of AuNPs $C_{NP} = 4 \times 10^{12}$ NPs/cc and of gold $C_{Au} = 46 \mu\text{g/mL}$. The increased particle size is responsible of the intensity of the plasmon band, which scales cubically with particle radius and linearly with particle concentration (Kreibig and Vollmer 1995). Also in this case, the inset of Fig. 2b shows a high resolution image of a pair of NPs, where the lattice planes are clearly visible. EDX microanalysis of this sample was also carried out and is reported in

Fig. 2c. Apart from the signal assigned to the copper grid, all the other bands clearly pertain to gold.

Lastly, the characteristics of batch B3 are shown in Fig. 3a, b. The resolution and intensity of the plasmon band is improved with respect to sample B1. This can be due to both the presence of some big NPs and to a reduced quantity of carbon on NPs surface. Indeed the presence of carbon can cause a non-negligible quenching of the plasmon resonance, due to its absorption in the visible spectral range. In this case, the best fit parameters of the Gaussian equivalent of the lognormal distribution were $2R = 2.4$ nm,

Fig. 3 **a** UV–Vis spectrum of sample B3 (red line) and theoretical fit (black line). OPL = 2 mm. **b** Typical TEM image of sample B3 with statistical distribution of particle size. (Color figure online)



$\sigma_- = 0.85$ nm, and $\sigma_+ = 2$ nm (Table 1). Fitting of the spectrum of Fig. 3a (red line) returned the values of $C_{NP} = 1 \times 10^{12}$ NP/cc and $C_{Au} = 53$ μ g/mL.

We also characterized the three batches by ζ -potential measurements. In all cases, we observed highly negative values (reported in Table 1), which indicate excellent stability of the samples.

In order to perform a characterization of AuNPs within the biological media, we mixed a small quantity of the colloids with culture medium. In the case of batch B1, we mixed 119.75 μ L of the colloid with 880.25 μ L of culture medium in order to achieve a concentration of gold of 8.8 μ g/mL. The obtained sample was characterized by TEM microscopy and by UV–Vis spectroscopy. Figure 4b shows a typical TEM image of the sample after mixing and the corresponding statistical distribution of NPs size.

Due to dilution the statistics was performed with a reduced number of particles with respect to Fig. 1 and it is, consequently, less reliable. However, it did not show significant changes, a part of some increase of average particle diameter and width of the distribution (see Table 1). The results of UV–Vis spectroscopy are reported in Fig. 4a. Green and red lines in Fig. 4a correspond to AuNPs/culture medium mixture and to culture medium, respectively, while thick blue line represents their difference and permits observation of a weak plasmon band at 523 nm and of the typical interband absorption of gold. Theoretical fit of the difference spectrum (thin blue line in Fig. 4a) permits evaluation of C_{Au} and of C_{NP} in the colloid. Although difference spectra are usually affected by large errors, the obtained results, which were $C_{Au} = 9.3$ μ g/mL and

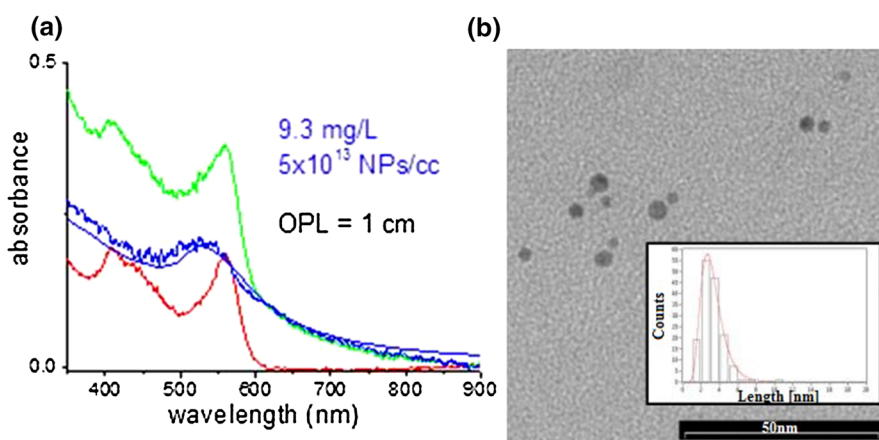


Fig. 4 **a** UV–Vis spectra of culture medium (green line), of the mixing of B1 with culture medium, corresponding to nominal 8.8 mg/L Au concentration (red line), and subtraction between the previous spectra (thick blue line). The thin blue line

represents the theoretical fit of the subtraction spectrum. OPL = 1 cm. **b** Typical TEM image and statistical distribution of particles size after mixing of sample B1 with culture medium. (Color figure online)

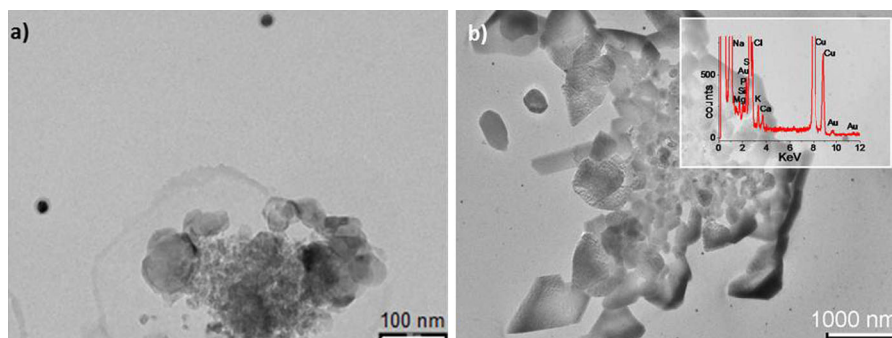


Fig. 5 Sample B2 after mixing with culture medium: **a** Typical TEM image and **b** Low magnification image and corresponding EDX spectrum (*inset*)

$C_{NP} = 5 \times 10^{13}$ NPs/cc, respectively, are in very good agreement with the expected values.

In the case of sample B2, we mixed it with culture medium, in order to obtain a $9.2 \mu\text{g/mL}$ solution of gold. Figure 5a shows a typical TEM image. Due to the dilution and to the initially low concentration of NPs, it was not possible to perform a reliable statistic of their size. However, the image shows clearly the presence of isolated spherical NPs, surrounded by a transparent shell, probably related to adsorption of some ligands of the medium. If a panoramic view of the sample is taken (*inset* of Fig. 5b), the coexistence of AuNPs and large irregular aggregates is clear. EDX inspection permitted to obtain the composition of these structures which, beyond Au, mainly contain Na, Cl, K, Mg, and P, as expected if the characteristics of the culture medium are taken into account.

As for sample B3, we diluted it in culture medium in order to obtain a $10.6 \mu\text{g/mL}$ concentration of gold. The results of TEM inspection were similar to those of sample B2, namely spherical AuNPs with a transparent shell and big structures which we again attributed to culture medium, thanks to EDX analysis. It is worth noticing that such transparent shell, also appearing in sample B2, is never observed in sample B1, suggesting a different surface nature and, hence, a different interaction with the environment.

Cell viability

The MTT assay was used to determine cell viability as shown in Fig. 6. A significant decrease in cell viability was observed in a dose-dependent manner (p value = 0.012) after B1 exposure to A549 cells, by

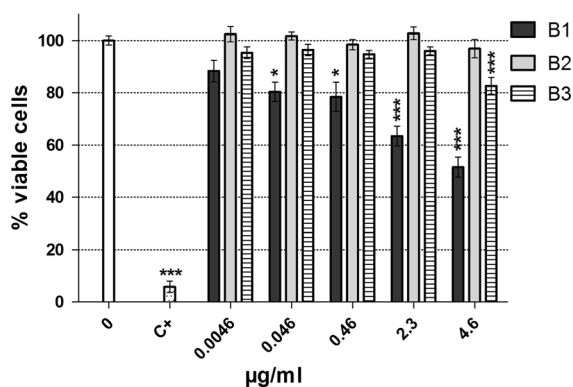


Fig. 6 MTT assay after 48 h exposure of A549 cells to different batches of AuNP. Cell viability results are presented as percentage of viability relative to untreated control. *Solid and error bars* represent the mean and the SEM, respectively ($n = 3$). C+: 1 mM sodium chromate. Statistical analysis was performed by one-way ANOVA and significant differences between untreated control and treated cells are indicated as follows: * $p < 0.05$, *** $p < 0.001$

reaching a 50 % cell death at $4.6 \mu\text{g/mL}$ exposure. No impairment of cell viability was seen after B2 treatment, while B3 treatment caused a significant reduction in cell viability (18 % of cell death) at the highest concentration.

Cytostasis and cytotoxicity

The cytokinesis-block proliferation index (CBPI), evaluated as the distribution of mononucleated, binucleated, and polynucleated cells, indicates the average number of cell cycles per cell and was determined for measuring cell proliferation (Fig. 7).

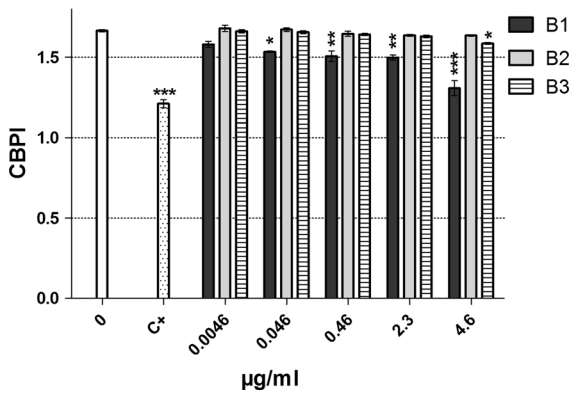


Fig. 7 CBPI index scored by CBMN Cyt assay. Data are presented as mean ± SEM (n = 3). C+: 0.10 µg/mL Mitomycin C. Statistical analysis was performed by one-way ANOVA and significant differences between untreated control and treated cells are indicated as follows: *p < 0.05, **p < 0.01, ***p < 0.001

Coherently with the results found in the cell viability assay, the proliferation rate decreased after exposing A549 cells to B1 in a dose-dependent manner (p value = 0.0152) and significantly at the highest tested mass concentration of B3 AuNP. B2 exposure did not show any cytostatic effect.

To elucidate mechanisms of noticed cell death, apoptotic and necrotic figures were morphologically evaluated by CBMN Cyt assay showing that cytotoxicity seems to occur mainly by necrotic events (Fig. 8). Apoptosis was significantly induced only at the highest mass concentration of B1 exposure while the percentages of necrotic events were significantly

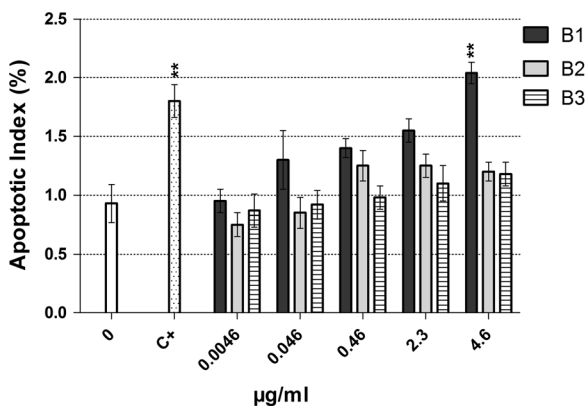


Fig. 8 Apoptotic (left) and necrotic (right) indices scored by CBMN Cyt assay. Data are presented as mean ± SEM (n = 3). C+: 0.10 µg/mL Mitomycin C. Statistical analysis was

different from the untreated control except for the lowest concentration of B1. The highest concentrations of B2 and B3 exposures showed a well-significant induction of necrotic events.

Genotoxicity

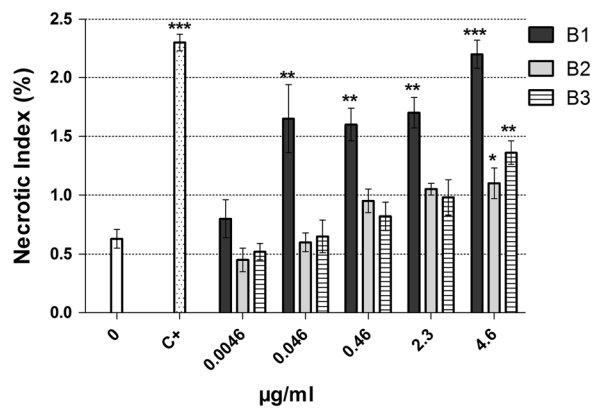
Figure 9 summarizes the micronuclei frequency, a biomarker of chromosomal damage and/or loss, found after exposing A549 cells to B1, B2, and B3 AuNPs. Only exposure at the two highest mass concentrations of B1 and the highest one of B3 showed a significant increase of micronuclei that were however induced in a dose-dependent manner after B1 exposure (p value = 0.006).

To better define genotoxic mechanisms induced by AuNPs, the frequencies of nucleoplasmic bridges and nuclear buds were also evaluated as biomarkers of reduced repair capacity as well as misrepair leading to chromosome rearrangement, and a measure of excess DNA that is being extruded from the nucleus, respectively (Fig. 10).

NPB frequency increased after quite all the B1 tested concentrations, and at 2.3 µg/mL of B2 exposure. NBUD formation was induced after all B1 exposures except the lowest one, and a significance was found also at 2.3 µg/mL of B2 exposure.

Discussion

The in vitro toxicity of AuNPs produced by chemical methods has been extensively studied so far, showing



performed by one-way ANOVA and significant differences between untreated control and treated cells are indicated as follows: *p < 0.05, **p < 0.01, ***p < 0.001

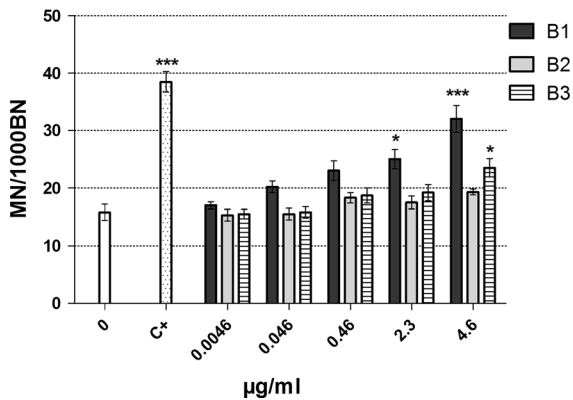


Fig. 9 Micronuclei frequencies scored by CBMN Cyt assay. Data are presented as mean \pm SEM ($n = 3$). C+: 0.10 $\mu\text{g}/\text{mL}$ Mitomycin C. Statistical analysis was performed by one-way ANOVA and significant differences between untreated control and treated cells are indicated as follows: * $p < 0.05$, *** $p < 0.001$

a degree of toxicity, related to the use of substances as reducing (e.g., citrate and ascorbic acid) and stabilizing agents (e.g., carboxylates, phosphines, amines, thiols). For instance, the presence of sodium citrate rather than the size of the AuNPs (mean diameter 11 and 25 nm), can affect both the cell viability (60–70 %) of human lung epithelial cell line A549 following 72 h exposure at 0.7 mM (142 $\mu\text{g}/\text{mL}$) and the cell proliferation in a dose- and time-dependent manner by reducing the proliferation rate to 50 % following 24 h exposure. (Uboldi et al. 2009). Analogously, for the same AuNPs, it was shown that

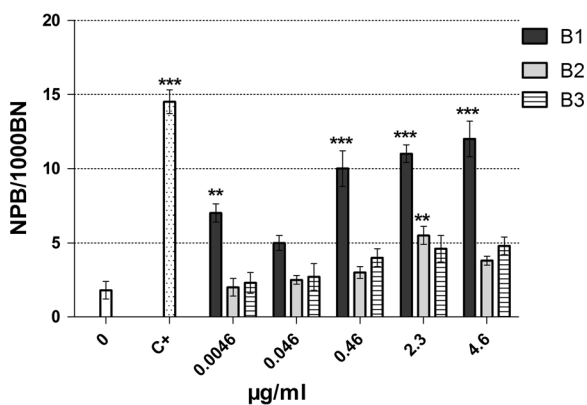
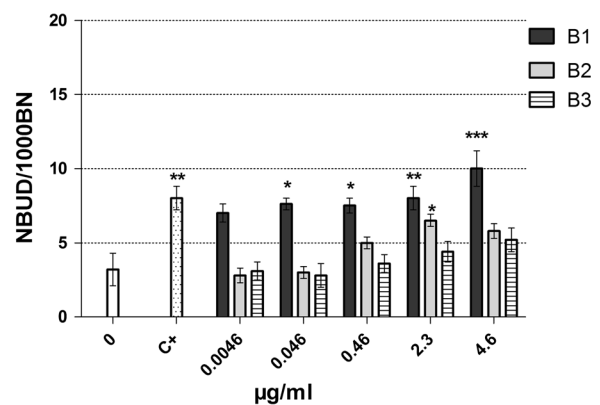


Fig. 10 Nucleoplasmic bridges (left) and Nuclear buds (right) frequencies scored by CBMN Cyt assay. Data are presented as mean \pm SEM ($n = 3$). C+: 0.10 $\mu\text{g}/\text{mL}$ Mitomycin C. Statistical analysis was performed by one-way ANOVA and

the amount of citrate on the particle surface rather than the size was correlated with impaired cell viability. HDMEC endothelial cells had a reduced cell viability by 25 % following 48 h exposure to 1000 μM (214 $\mu\text{g}/\text{mL}$) of both 11 and 25 nm sized NPs as well as a reduced cell proliferation by 20 % after exposure to 50 μM (10 $\mu\text{g}/\text{mL}$) (Freese et al. 2012). The importance of the surface properties to increase the biocompatibility of AuNPs was emphasized showing that, in spite of the absence of cytotoxicity, ~ 20 nm spherical citrate-coated AuNPs induced DNA damage, while 11-mercaptopundecanoic acid-coated AuNPs did not, as assessed by comet assay in human liver HepG2 cells (Fraga et al. 2013). AuNPs with diameters ranging from 7 to 20 nm and capped with either sodium citrate or polyamidoamine dendrimers (PAMAM) interact with HepG2 cells and peripheral blood mononuclear cells and exhibit cyto- and genotoxicity even at very low concentrations (1.0 μM , i.e., 0.2 $\mu\text{g}/\text{mL}$) (Paino et al. 2012). The presence of 13 and 45 nm citrate-coated AuNPs in adipose-derived stromal cells resulted in increased population doubling times, decreased cell motility, and cell-mediated collagen contraction (Mironava et al. 2014). Furthermore, differently sized citrated-AuNPs (5 and 15 nm) significantly decreased the cell viability of human primary lymphocytes and Raw264.7 murine macrophages by 20–30 % following 24 h exposure to 10 $\mu\text{g}/\text{mL}$, inhibited cell proliferation via apoptosis, and induced aneuploidogenic effects as well as DNA oxidation (Di Bucchianico et al. 2014). Polyethylene



significant differences between untreated control and treated cells are indicated as follows: * $p < 0.05$, ** $p < 0.01$, *** $p < 0.001$

glycol (PEG)-functionalized AuNPs, with average sizes of 4.5, 13, and 30 nm, have the potential to affect the primary function of human erythrocytes in a size-dependent manner, by decreasing their deformability and oxygen-delivering ability due to the interaction between PEGylated AuNPs and erythrocytes membranes (He et al. 2014).

Beside in vitro studies showing that surface chemistry of AuNPs plays a crucial role in determining cyto- and genotoxicity, the importance of physicochemical characteristics of AuNP surface in determining toxicity was investigated also in vivo. For instance, using an embryonic zebrafish model it was showed that the surface functionalization with a monolayer of TMAT (N,N,N-trimethylammoniummethanethiol) cationic ligand dictated toxicity outcomes by increasing apoptotic responses and altering expression of transcript factors that continue to behavioral and neuronal damage in the development of zebrafish (Kim et al. 2013). The long-term effect of acute exposure to differently functionalized AuNPs (such as the negatively charged 2-mercaptoethanesulfonic acid or neutral 2-(2-(2-mercaptoethoxy)ethoxy)ethanol ligands or positively charged TMAT) was investigated during embryonic development in a zebrafish model, showing that both negatively and positively charged AuNPs exposed embryos exhibited hypolocomotor activity and affected larval behavior, with behavioral effects persisting into adulthood (Truong et al. 2012).

In contrast to the above discussed investigations, our PLAL-prepared AuNPs are surfactant-free. Concerning reaction by-products, they can be completely absent, as in the case of sample B2, which was obtained in pure deionized water, or present in different amounts, as in the case of B1 and B3, that were prepared in pure acetone. As a matter of fact, laser irradiation can induce some degradation of acetone close to AuNPs surface, causing both formation of amorphous carbon and surface adsorption of enolate ions. Previous investigations reported by some of us showed that this effect is expected to be considerably reduced under 1064 nm irradiation (fabrication conditions for sample B3), with respect to 532 nm irradiation (fabrication conditions for sample B1) (Giorgetti et al. 2012). Raman tests performed on a sample obtained in the same experimental conditions as B1 permitted rather easy detection of carbon and enolate, while no trace of such surface contaminants could be detected in colloids obtained by following the

same experimental parameters as sample B3. This point is also confirmed by ζ -potential data of B1, B2, and B3 (reported in Table 1), showing how the ζ -potential of the three colloids, which is related to their surface charge, gets closer to 0 as long as the expected amount of surface carbon increases, going from -43 mV for the completely carbon-free B2 sample to -23 mV for B1. Regarding size, samples B1 and B3 are comparable, apart from some differences in dispersivity, where B3 statistical distribution of diameters being a bit larger, especially on the side of big values. Therefore, the comparison between the results corresponding to B1 and B3, having comparable size, can highlight the effect of carbon/enolate coating on NPs cyto- and genotoxic behavior. Analogously, the considerable size difference between samples B2 and B3 and the low carbon/enolate content of B3 can elucidate the role of NPs size on the cyto- and genotoxic behavior. In this sense, it is worth noticing that sample B2 contains a non-negligible amount of NPs larger than 12 nm and that, for fixed Au concentrations, the number of AuNPs per unit volume in B2 is 20–50 times smaller than in B1 or B3.

In our study, AuNPs showed different degrees of cytotoxicity and genotoxicity, depending on surface chemistry properties, size, and dispersivity. When the AuNPs were prepared by laser ablation in deionized water (sample B2), no impairment of cytostasis and cytotoxicity and no signs of genotoxicity were highlighted in the explored Au concentration range. In contrast, AuNPs produced by PLAL in pure acetone and then transferred into deionized water showed some toxicity. In particular, sample B1, which contained the smallest NPs and the largest amount of amorphous carbon and enolate ions, showed up to 50 % reduced cell viability following 48 h exposure to 4.6 $\mu\text{g}/\text{mL}$ as well as significant dose-dependent cytostasis and genotoxicity, which were higher than those observed with sample B3 (up to 20 % reduced cell viability), namely a sample with comparable average NP size and reduced amount of surface contaminants.

In summary, PLAL-prepared AuNPs in water did not show any significant toxicity up to the tested concentration values. When compared to the acetone-prepared samples, for fixed values of C_{Au} , the lack of toxicity can be due to both extreme surface cleanliness and purity of the solution and to larger size and consequently lower C_{NP} . However, the comparison

between B1 and B3 suggests that NPs toxicity originates mainly from carbon residues, as expected on the basis of previous investigation on the toxicity of carbon NPs (Panessa-Warren et al. 2006). That toxicity can be preferentially related to a different surface nature and is also compatible with the different ζ -potential value exhibited by sample B1 and by the absence of the halo, which on the contrary appears around B2 and B3 AuNPs in the culture medium, and which suggests a different biological reactivity.

Conclusions

We presented a cyto- and genotoxicity study of PLAL-prepared AuNPs on adenocarcinoma epithelial A549 cells. Thanks to the absence of surfactants, that is permitted by the preparation method, we could isolate the contribution of nanosized Au from that of capping agents, which is not straightforward when AuNPs are obtained by current wet chemical methods. Although some results on cytotoxicity of PLAL-prepared AuNPs were already available in the literature (Salmaso et al. 2009; Taylor et al. 2010), our study includes evaluation of genotoxic effects and our results span over a broader concentration interval. Moreover we used very small AuNPs and compared batches exhibiting different surface properties, due to the different ablation conditions, obtaining a more comprehensive overview of their potential effects on human cells.

Briefly, we demonstrated that, within the explored size range, poor surface cleanliness can affect the toxic effect of AuNPs, as observed for the case of colloids obtained in pure acetone and then transferred into deionized water. In particular, the occurrence of some degree of acetone decomposition under laser irradiation and subsequent formation of carbon on the surface of the NPs confirmed the already reported toxic effect of carbon traces on living tissues (Panessa-Warren et al. 2006). In contrast, in the case of AuNPs prepared directly by PLAL in pure deionized water, we did not observe any significant signs of cytotoxicity, cytostasis, and/or genotoxicity up to concentrations of the order of 5 $\mu\text{g}/\text{mL}$.

Acknowledgments This study was partially funded by the European Commission's Seventh Framework Programme (FP7/2007-2013) under grant agreement No. FP7-280716 Project Name Sanowork (<http://www.sanowork.eu>).

Conflict of interest The authors report no conflicts of interest in this work.

References

- Alkilany AM, Murphy CJ (2010) Toxicity and cellular uptake of gold nanoparticles: what we have learned so far? *J Nanopart Res* 12(7):2313–2333. doi:10.1007/s11051-010-9911-8
- Balansky R, Longobardi M, Ganchev G, Iltcheva M, Nedyalkov N, Atanasov P, Toshkova R, De Flora S, Izzotti A (2013) Transplacental clastogenic and epigenetic effects of gold nanoparticles in mice. *Mutat Res* 751–752:42–48. doi:10.1016/j.mrfmmm.2013.08.006
- Connor EE, Mwamuka J, Gole A, Murphy CJ, Wyatt MD (2005) Gold nanoparticles are taken up by human cells but do not cause acute cytotoxicity. *Small* 1(3):325–327. doi:10.1002/sml.200400093
- Correard F, Maximova K, Estève MA, Villard C, Roy M, Al-Kattan A, Sentis M, Gingras M, Kabashin AV, Braguer D (2014) Gold nanoparticles prepared by laser ablation in aqueous biocompatible solutions: assessment of safety and biological identity for nanomedicine applications. *Int J Nanomed* 9(1):5415–5430. doi:10.2147/IJN.S65817
- Davis ME, Zuckerman JE, Choi CHJ et al (2010) Evidence of RNAi in humans from systematically administered siRNA via targeted nanoparticles. *Nature* 464:1067–1070. doi:10.1038/nature08956
- Demartini A, Alloiso M, Cuniberti C, Dellepiane G, Jadhav SA, Thea S, Giorgetti E, Gellini C, Muniz-Miranda M (2009) Polydiacetylene functionalized noble metal nanocages. *J Phys Chem C* 113:19475–19481. doi:10.1021/jp905787h
- Di Bucchianico S, Fabbri MR, Misra SK, Valsami-Jones E, Berhanu D, Reip P, Bergamaschi E, Migliore L (2013) Multiple cytotoxic and genotoxic effects induced in vitro by differently shaped copper oxide nanomaterials. *Mutagenesis* 28(3):287–299. doi:10.1093/mutage/get014
- Di Bucchianico S, Fabbri MR, Cirillo S, Uboldi C, Gilliland D, Valsami-Jones E, Migliore L (2014) Aneuploidogenic effects and DNA oxidation induced in vitro by differently sized gold nanoparticles. *Int J Nanomed* 9:2191–2204. doi:10.2147/IJN.S58397
- Dreaden EC, Alkilany AM, Huang X, Murphy CJ, El-Sayed MA (2012) The golden age: gold nanoparticles for biomedicine. *Chem Soc Rev* 40:2740–2779. doi:10.1039/c1cs15237h
- Dykman L, Khlebtsov N (2012) Gold nanoparticles in biomedical applications: recent advances and perspectives. *Chem Soc Rev* 41:2256–2282. doi:10.1039/c1cs15166e
- Fenech M (2007) Cytokinesis-block micronucleus cytome assay. *Nat Protoc* 2(5):1084–1104. doi:10.1038/nprot.2007.77
- Fraga S, Faria H, Soares ME, Duarte JA, Soares L, Pereira E, Costa-Pereira C, Teixeira JP, de Lourdes Bastos M, Carmo H (2013) Influence of the surface coating on the cytotoxicity, genotoxicity and uptake of gold nanoparticles in human HepG2 cells. *J Appl Toxicol* 33(10):1111–1119. doi:10.1002/jat.2865

- Freese C, Uboldi C, Gibson MI, Unger RE, Weksler BB, Romero IA, Couraud PO, Kirkpatrick CJ (2012) Uptake and cytotoxicity of citrate-coated gold nanospheres: comparative studies on human endothelial and epithelial cells. *Part Fibre Toxicol* 9:23. doi:[10.1186/1743-8977-9-23](https://doi.org/10.1186/1743-8977-9-23)
- Giammanco F, Giorgetti E, Marsili P, Giusti A (2010) Experimental and theoretical analysis of photofragmentation of Au nanoparticles by picosecond laser radiation. *J Phys Chem C* 114:3354–3363. doi:[10.1021/jp908964t](https://doi.org/10.1021/jp908964t)
- Giorgetti E, Muniz-Miranda M, Margheri G, Giusti A, Sottini S, Alloisio M, Cuniberti C, Dellepiane G (2006) UV polymerisation of self-assembled monolayers of a novel diacetylene on silver: a spectroscopic analysis by surface plasmon resonance and by surface enhanced Raman scattering. *Langmuir* 22(3):1129–1134. doi:[10.1021/la0514157](https://doi.org/10.1021/la0514157)
- Giorgetti E, Giusti A, Giammanco F, Marsili P, Laza S (2009) Dendrimer-capped nanoparticles prepared by picosecond laser ablation in liquid environment. *Molecules* 14(9):3731–3753. doi:[10.3390/molecules14093731](https://doi.org/10.3390/molecules14093731)
- Giorgetti E, Giammanco F, Marsili P, Giusti A (2011) Effect of ps post-irradiation on colloidal suspensions of differently capped AuNPs. *J Phys Chem C* 115:5011–5020. doi:[10.1021/jp108042m](https://doi.org/10.1021/jp108042m)
- Giorgetti E, Muniz-Miranda M, Marsili P, Scarpellini D, Giammanco F (2012) Stable gold nanoparticles obtained in pure acetone by laser ablation with different wavelengths. *J Nanopart Res* 14(1):648. doi:[10.1007/s11051-011-0648-9](https://doi.org/10.1007/s11051-011-0648-9)
- Giusti A, Giorgetti E, Laza S, Marsili P, Giammanco F (2007) Multiphoton fragmentation of PAMAM G5-capped-gold nanoparticles induced by picosecond laser irradiation at 532 nm. *J Phys Chem C* 111:14984–14991. doi:[10.1021/jp072611k](https://doi.org/10.1021/jp072611k)
- Haiss W, Thanh NT, Aveyard J, Fernig DG (2007) Determination of size and concentration of gold nanoparticles from UV-Vis spectra. *Anal Chem* 79:4215–4221. doi:[10.1021/ac0702084](https://doi.org/10.1021/ac0702084)
- He Z, Liu J, Du L (2014) The unexpected effect of PEGylated gold nanoparticles on the primary function of erythrocytes. *Nanoscale* 6(15):9017–9024. doi:[10.1039/c4nr01857e](https://doi.org/10.1039/c4nr01857e)
- Jeong M, Park JM, Lee EJ, Cho YS, Lee C (2013) Cytotoxicity of ultra-pure TiO₂ and ZnO nanoparticles generated by laser ablation. *Bull Korean Chem Soc* 34(11):3301–3306. doi:[10.5012/bkcs.2013.34.11.3301](https://doi.org/10.5012/bkcs.2013.34.11.3301)
- Kim YS, Kim KK, Shin S, Park SM, Hah SS (2012) Comparative toxicity studies of ultra-pure Ag, Au Co, and Cu nanoparticles generated by laser ablation in biocompatible aqueous solution. *Bull Korean Chem Soc* 33(10):3265–3268. doi:[10.5012/bkcs.2012.33.10.3265](https://doi.org/10.5012/bkcs.2012.33.10.3265)
- Kim KT, Zaikova T, Hutchison JE, Tanguay RL (2013) Gold nanoparticles disrupt zebrafish eye development and pigmentation. *Toxicol Sci* 133(2):275–288. doi:[10.1093/toxsci/kft081](https://doi.org/10.1093/toxsci/kft081)
- Kreibig U, Vollmer M (1995) Optical properties of metal clusters., Springer series in Materials Science Springer-Verlag, Berlin
- Li JJ, Lo SL, Ng CT, Gurung RL, Hartono D, Hande MP, Ong CN, Bay BH, Yung LY (2011) Genomic instability of gold nanoparticle treated human lung fibroblast cells. *Biomaterials* 32(23):5515–5523. doi:[10.1016/j.biomaterials.2011.04.023](https://doi.org/10.1016/j.biomaterials.2011.04.023)
- Liu ZA, Li XL, Tabakman SM, Jiang KL, Fan SS, Dai HJ (2008) Multiplexed multicolor Raman imaging of live cells with isotopically modified single walled carbon nanotubes. *J Am Chem* 130:13540–13541. doi:[10.1021/ja806242t](https://doi.org/10.1021/ja806242t)
- Liu Z, Wu Y, Guo Z, Liu Y, Shen Y, Zhou P, Lu X (2014) Effects of internalized gold nanoparticles with respect to cytotoxicity and invasion activity in lung cancer cells. *PLoS One* 9(6):e99175. doi:[10.1371/journal.pone.0099175](https://doi.org/10.1371/journal.pone.0099175)
- McCarthy TD, Karellas P, Henderson SA et al (2005) Dendrimers as drugs: discovery and preclinical and clinical development of dendrimer-based microbicides for HIV and STI prevention. *Mol Pharm* 2:312–318. doi:[10.1021/mp050023q](https://doi.org/10.1021/mp050023q)
- Mironava T, Hadjiargyrou M, Simon M, Rafailovich MH (2014) Gold nanoparticles cellular toxicity and recovery: adipose derived stromal cells. *Nanotoxicology* 8(2):189–201. doi:[10.3109/17435390.2013.769128](https://doi.org/10.3109/17435390.2013.769128)
- Paino IM, Marangoni VS, de Oliveira Rde C, Antunes LM, Zucolotto V (2012) Cyto and genotoxicity of gold nanoparticles in human hepatocellular carcinoma and peripheral blood mononuclear cells. *Toxicol Lett* 215(2):119–125. doi:[10.1016/j.toxlet.2012.09.025](https://doi.org/10.1016/j.toxlet.2012.09.025)
- Pan Y, Leifert A, Ruau D, Neuss S, Bornemann J, Schmid G, Brandau W, Simon U, Jahnen-Dechent W (2009) Gold nanoparticles of diameter 1.4 nm trigger necrosis by oxidative stress and mitochondrial damage. *Small* 5(18):2067–2076. doi:[10.1002/sml.200900466](https://doi.org/10.1002/sml.200900466)
- Panessa-Warren BJ, Warren JB, Wong SS, Misewich JA (2006) Biological cellular response to carbon nanoparticle toxicity. *J Phys* 18:S2185–S2201. doi:[10.1088/0953-8984/18/33/S34](https://doi.org/10.1088/0953-8984/18/33/S34)
- Peer D, Karp JM, Hong S, Farokhzad OC, Margalit R, Langer R (2007) Nanocarriers as an emerging platform for cancer therapy. *Nat Nanotechnol* 2(12):751–760. doi:[10.1038/nnano.2007.387](https://doi.org/10.1038/nnano.2007.387)
- Resch-Genger U, Grabolle M, Cavaliere-Jaricot S, Nitschke R, Nann T (2008) Quantum dots versus organic dyes as fluorescent labels. *Nat Methods* 5:763–775. doi:[10.1038/nmeth.1248](https://doi.org/10.1038/nmeth.1248)
- Salmaso S, Caliceti P, Amendola V, Meneghetti M, Magnusson JP, Pasparakisc G, Alexander C (2009) Cell up-take control of gold nanoparticles functionalized with a thermoresponsive polymer. *J Mater Chem* 19:1608–1615. doi:[10.1039/B816603J](https://doi.org/10.1039/B816603J)
- Schaeublin NM, Braydich-Stolle LK, Maurer EI, Park K, MacCuspie RI, Afroz AR, Vaia RA, Saleh NB, Hussain SM (2012) Does shape matter? Bioeffects of gold nanomaterials in a human skin cell model. *Langmuir* 28(6):3248–3258. doi:[10.1021/la204081m](https://doi.org/10.1021/la204081m)
- Söderstjerna E, Bauer P, Cedervall T, Abdshill H, Johansson F, Johansson UE (2014) Silver and gold nanoparticles exposure to in vitro cultured retina—studies on nanoparticle internalization, apoptosis, oxidative stress, glial- and microglial activity. *PLoS One* 9(8):e105359. doi:[10.1371/journal.pone.0105359](https://doi.org/10.1371/journal.pone.0105359)
- Soenen SJ, Manshian B, Montenegro JM, Amin F, Meermann B, Thiron T, Cornelissen M, Vanhaecke F, Doak S, Parak WJ, De Smedt S, Braeckmans K (2012) Cytotoxic effects of gold nanoparticles: a multiparametric study. *ACS Nano* 6(7):5767–5783. doi:[10.1021/mn301714n](https://doi.org/10.1021/mn301714n)

- Sperling RA, Rivera Gil P, Zhang F, Zanella M, Parak WJ (2008) Biological applications of gold nanoparticles. *Chem Soc Rev* 7:1896–1908. doi:[10.1039/b712170a](https://doi.org/10.1039/b712170a)
- Taylor U, Klein S, Petersen S, Kues W, Barcikowski S, Rath D (2010) Nonendosomal cellular uptake of ligand-free, positively charged gold nanoparticles. *Cytom A* 77(5):439–446. doi:[10.1002/cyto.a.20846](https://doi.org/10.1002/cyto.a.20846)
- Trigari S, Rindi A, Margheri G, Sottini S, Dellepiane G, Giorgetti E (2011) Synthesis and modelling of gold nanostars with tunable morphology and extinction spectrum. *J Mater Chem* 21:6531–6540. doi:[10.1039/C0JM04519E](https://doi.org/10.1039/C0JM04519E)
- Truong L, Sali KS, Miller JM, Hutchison JE, Tanguay RL (2012) Persistent adult zebrafish behavioral deficits results from acute embryonic exposure to gold nanoparticles. *Comp Biochem Physiol C* 155(2):269–274. doi:[10.1016/j.cbpc.2011.09.006](https://doi.org/10.1016/j.cbpc.2011.09.006)
- Turkevich J, Stevenson PC, Hillier J (1953) The formation of colloidal gold. *J Phys Chem* 57(7):670–673. doi:[10.1021/j150508a015](https://doi.org/10.1021/j150508a015)
- Uboldi C, Bonacchi D, Lorenzi G, Hermanns MI, Pohl C, Baldi G, Unger RE, Kirkpatrick CJ (2009) Gold nanoparticles induce cytotoxicity in the alveolar type-II cell lines A549 and NCIH441. *Part Fibre Toxicol* 22:6–18. doi:[10.1186/1743-8977-6-18](https://doi.org/10.1186/1743-8977-6-18)
- Zeng H, Du XW, Singh SC, Kulinich SA, Yang S, He J, Cai W (2012) Nanomaterials via laser ablation/irradiation in liquid: a review. *Adv Funct Mater* 22:1333–1353. doi:[10.1002/adfm.201102295](https://doi.org/10.1002/adfm.201102295)